Indian Journal of Pure & Applied Physics
Vol. 62, September 2024, pp. 825-833
DOI: 10.56042/ijpap.v62i9.8708

Design and Performance Investigation of Low-Cost, Highly Sensitive Ag-Ta_2O_5 Coated PCF-Based SPR Sensor

Sudhir Kumar* & Dilip Kumar

Department of Electronics and Communication Engineering, SLIET Longowal, Punjab 148 106, India

Received 12 February 2024; accepted 1 August 2024

This paper uses numerical investigation to present an efficient photonic crystal fiber (PCF) surface plasmon resonance (SPR) sensor. The proposed sensor is simulated and modelled by the finite element method (FEM). The plasmonic and analyte layers are utilized on the fiber's exterior to ease practical implementation. Additionally, the designed sensor contains all the circular air holes, making it simpler and easier to fabricate using currently available techniques. Silver (Ag) and tantalum pentaoxide (Ta_2O_5) are used as plasmonic materials for surface plasmon generations and to achieve smooth coupling. The sensor achieves the maximum wavelength sensitivity of 22860 nm/RIU and amplitude sensitivity of 1758 1/RIU. Moreover, the sensor shows a wide refractive range of chemical sensing capabilities within 1.375-1.400. Due to the broad RI detection range, the proposed sensor can detect various biological cells, biochemicals, and food additives, making this sensor applicable in medical applications and food quality control.

Keywords: Photonic crystal fiber; Surface plasmon resonance; Optical communication

1 Introduction

PCFs, because of their flexible design and superior optical properties, are being investigated for a range of optical communication applications: four-wave mixing[1], signal switcher[2], ultra-short soliton pulse transmission[3], optical code division multiplexer[4], optical parametric amplifier[5], fibre laser[6] *etc*. Besides optical communication, this fibre can be utilized in various sensing applications like chemical and biosensing[7]. The analyte may be detected by the interaction of light with the analyte after the desired analyte has been introduced into a certain number of airholes and light has been guided through it[8]. Scientists and researchers have recently reported PCFs by employing SPR techniques in sensing applications[9]. Initially, the SPR technique was utilized by prism-based configuration (known as Otto configuration)[10], were used where a dielectric (analyte) layer parted the prism and metal layer; this configuration quite refined as it is required to sustain a limited gap between the layers. Due to this limitation, the Otto configuration was improved by the Kretschmann arrangement[11], where the prism and plasmonic layers were in straight contact. This configuration was widely used for the SPR sensing. Prism-based SPR sensors (Kretschmann setup) have strong performance, but because of their bulky configuration and necessary optical and mechanical components, they are not as good as they could be[12]. These specifications restrict how these devices may be optimized and used in real-world point-of-care situations. Conventional optical fibre-based SPR sensors were used as an alternative to prism-based SPR sensors[13]. Fibre optic probes based on transmission and reflection have been described for numerous sensing applications[14,15]. These sensors used the total internal reflection (TIR) phenomenon to confine the light for sensing purposes through the SPR technique. Sensing performance through this method is limited by the lack of characteristics such as single-mode guiding, flexibility to guide light in a specific direction, bending, dispersion[16], *etc*. PCFs exhibit design flexibility and superior optical properties[17]. Because of these extraordinary characteristics, PCF-based SPR sensors overcome the limitations of prism and optical fibre-based sensors. These particular sensors put an analyte over the plasmonic material-coated detecting area. Achieving the SPR condition results in the optical stimulation of surface plasmonpolaritons (SPPs). A label-free detection approach for tracking instantaneous biomolecular measures is the SPR biosensing technology[18].

SPR sensors are widely used because of their high sensitivity, efficacy, instantaneous detection, efficient light confinement, and ease of use. SPR sensors based

*Corresponding author: (E-mail: 1294kumar@gmail.com)

on PCFs have been extensively studied for humidity[19], pressure, strain, temperature[20], and refractive index (RI)[21] sensing. Researchers have made meaningful improvements in PCF-based SPR sensors and their applications in recent years. The requirement of a metallic coating is one of the practical limitations of SPR sensors[21]. This would result in fabrication difficulty for PCF-based SPR sensors. Various PCF SPR sensor designs have been published to streamline the progression of depositing metallic layers inside or outside of fiber structures[22]. The sesensors are categorized as externally and internally coated metal films[23,24]. From a fabrication perspective, the selective deposition of a thin metal film within the microairholes is a complex procedure. Metal coating outside the fiber has been suggested to circumvent the metal coating and liquid analyte infiltration within the air holes. The outside side of the fiber structure has a metal layer and a sensing medium, which improves the convenience of the sensing mechanism[25]. PCF design's practicability is crucial to any learning in this field. Like a D-shaped PCF structure, a side of the PCF is polished to a suitable space from the center. Various shapes of airholes, including square (amplitude sensitivity = 906 1/RIU)[26] and elliptical (wavelength sensitivity = 116, 500 nm/RIU)[27] *etc*., are complicated to fabricate using the traditional stack-and-draw procedure used to create photonic crystal fibers. Even though these sensors' achieved sensitivity is higher than the other suggested sensor's, they should not be used if manufacture is not feasible. Additionally, to facilitate and increase the viability of the fabrication process, all air holes should have the same diameter.

Many PCF-based SPR sensors that utilize graphene, TiO_2, and Ta_2O_5 layers have been reported; their effects on sensitivity have been investigated[28-30]. Silver was found to be more appropriate for that particular structure after a numerical comparison of Gold and Silver on the same PCF structure was examined[31]. This has attracted the attention of researchers and led them towards low-cost sensor design.

This work presents a cost-effective, fabrication-feasible Ag-Ta_2O_5 externally coated PCF-based SPR sensor. Also, the effects of plasmonic materials combination Au-TiO_2, Ag-TiO_2, Cu-TiO_2, or Al-TiO_2 and Au-Ta_2O_5, Ag-Ta_2O_5, Cu-Ta_2O_5 or Al-Ta_2O_5 are also investigated for the same design and analyte. Additionally, the comparison is made based on the performance parameters. This sensor can be utilized for a wide range (1.375-1.400)of RI detection in chemical and bio-sensing applications, especially in pharmaceuticals and food quality control. A FEM-based mode solver solves dispersion relations and computation losses[32]. The proposed sensor's PCF fiber consists of a solid core and cladding part; silica is used as the background material. Plasmonic material layers, analyte, and perfectly matched layer (PML) are placed outside the fiber. The cladding portion is formed by using two layers of airholes. The arrangement is made octagonally in the inner layer, while in the outer layer, airholes are arranged circularly. Two circular airholes are removed along the y-axis from the second cladding layer to focus the most source of the evanescent field at the appropriate sides, resulting in sensitivity enhancement. All the circular airholes are utilized to make sensor fabrication feasible, facilitating the fabrication of PCF using the stack and draw process[33].

Moreover, all the plasmonic material layers are created circularly and placed outside the fiber. Furthermore, chemical vapour procedures are presented to deposit these material layers[34,35]. The analyte layer is also formed circularly to make the sensor more simple.

2 Structure Design

The design of the proposed PCF-based SPR sensor with a solid core, two layers of cladding airholes, and two plasmonic material layers is shown in Fig. 1(a).

The analyte circular layer is created to permit the selective filling of the chemical analyte. The size of the pitch P (centre-to-centre distance) is 2 μm, the diameter of the core is d_c=1.5P, the airhole diameter of the first cladding layer of d=0.5P and the diameter of the outer cladding layer is d_1=0.75P is used. Fused silica is the primary background material used in constructing this structure, and Sellmeier's equation 1 determines the material adsorption of this material. The first 60nm Silver (Ag)plasmonic layer is engaged to smooth the SPPs. The titanium dioxide (TiO_2) or tantalum pentaoxide(Ta_2O_5) with a thickness of 30 nm is utilized separately with Silver as the second plasmonic layer to avoid Silver's low environmental stability and oxidation.

Furthermore, a substantial quantity of surface electrons are released by the TiO_2 layer, which effectively draws the field away from the core and promotes a strong interaction with the plasmonic mode. The Ta_2O_5 layer avoids oxidation of first-layer

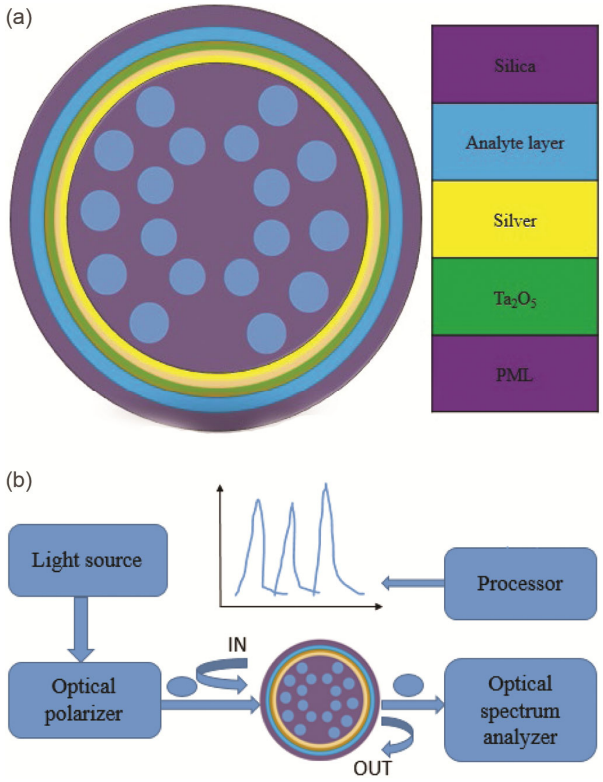

Fig. 1 — (a) Transverse view of the proposed sensor (b) Proposed sensor's experimental setup

plasmonic materials, enhancing sensitivity. The modelling and numerical mode analysis are done using COMSOL Multiphysics software. This is accomplished using the electromagnetic wave frequency domain (EWFD) analyzer and the RF module[32].

$$n_{SiO_2} = \sqrt{(1 + (a_1 l^2)/(l^2 - b_1) + (a_2 l^2)/(l^2 - b_2) + (a_3 l^2)/(l^2 - b_3))} \quad \ldots(1)$$

Here, n_{SiO_2} is the RI of silica, and l is the operating wavelength, while a_1, a_2, a_3, and b_1, b_2, and b_3 are the Sellmeiers coefficients[36]. The values of these coefficients are illustrated in Table 1.

The proposed PCF-based SPR sensor exhibits high sensitivity because the materials TiO_2 and Ta_2O_5 used for the second plasmonic layer are of high refractive indices, which improves the excitation of SPPs[37], which leads to the generation of a significant number of surface electrons at the metal-dielectric interface.

$$n_{TiO_2} = \sqrt{(5.913 + (2.441)/(l^2 - 0.803))} \quad \ldots(2)$$

The RI of TiO_2 and Ta_2O_5[36] are determined by Eqs 2 & 3, respectively.

$$n_{Ta_2O_2} = 1.88 + \left(178.4 + \frac{100}{l^2}\right) + (52.7 + \frac{10^7}{l^4}) \quad \ldots(3)$$

Table 1 — Sellmeier's coefficients

a_1	a_2	a_3	b_1	b_2	b_3
0.696166	0.407942	0.897479	0.004679	0.013512	97.934002

n_{TiO_2} is the RI of TiO_2, $n_{Ta_2O_5}$ is the RI of Ta_2O_5, and l represents the operating wavelength.

The dielectric constants of the first layer of plasmonic materials are determined by the Drude-Lorentz equations described in[19,38]. The liquid sample is employed in the circular analyte channel. An analyte is assessed by entering a loss peak under SPR conditions. The peak amplitude dissimilarity or wavelength shifts with RI variation are utilized as performance variations of the sensor. The arrangement of the experimental[39] system can be implemented, as shown in Fig. 1(b).

3 Results and Analysis

This part presents and investigates the results based on the Amplitude sensitivity (AS) and wavelength sensitivity (WS) parameters. Additionally, the effect of the thickness of plasmonic material layers is also analyzed. Furthermore, loss spectra concerning wavelength for various detected analytes, fabrication feasibility, and comparison of Ag-coated sensors with Au, Cu, and Al-coated sensors are also presented.

3.1 Sensing mechanism and field distribution

The core, SPP, and coupling modes for the proposed sensor for RI=1.39 are illustrated in Fig. 2(b). Plasmonic materials are used to achieve SPP mode. Two air holes from the second cladding layer are removed so that the maximum amount of light reaches through the plasmonic material, which excites surface electrons. These electrons produce a surface plasmonic wave covered across the metal-dielectric interface. When the surface electrons frequency and the incident light frequencies are matched, the particular condition is known as the phase matching condition; the corresponding frequency is known as the resonant frequency. For the core mode, light energy is concentrated in the core region. In SPP mode, a substantial quantity of energy is concentrated at the surface of plasmonic material due to the SPR phenomenon. In the coupling mode, most of the energy of the core mode is transferred to the SPP mode. This mode is achieved at the resonant frequency when the real part of RI of the core mode and SPP mode becomes equivalent. The resonant wavelength and phase matching condition are altered when the RI of the analyte changes. The change in resonant wavelength detects the unknown analyte[40].

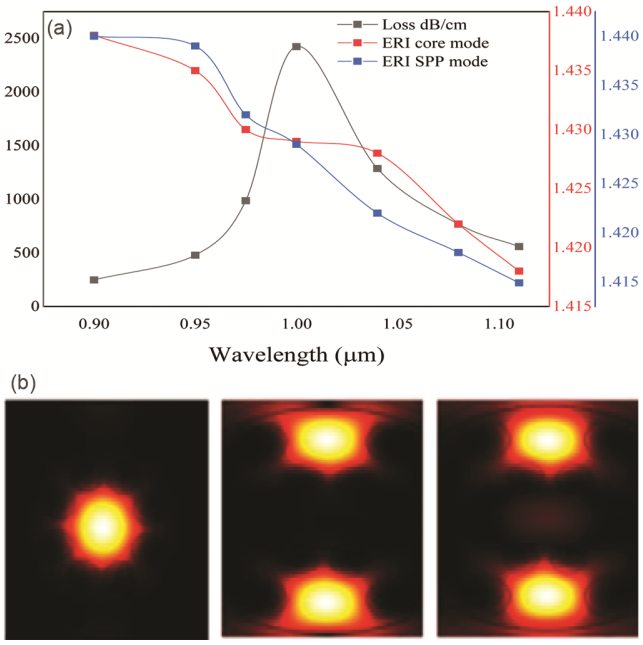

Fig. 2 — (a) Dispersion relation between the guided modes (b) Light propagation in different guided modes

3.2 Confinement loss

The phase-matching condition is calculated based on the core mode's confinement loss (CL). At this condition, a loss peak is achieved. CL is calculated by the imaginary part of the effective refractive index (ERI). The loss spectra and numerical calculation of CL are determined by Fig. 2(a) and Eq. 4[41]. Moreover, the loss spectra for various RIs are illustrated in Fig. 3.

$$CL = \frac{8.686.imag(n_{eff}).10^4}{l.log(10)} dB/cm \quad \ldots(4)$$

Here, Imag(n_{eff}) It is the imaginary part of ERI of the core mode, l is the operating wavelength, and dB/cm is the unit of CL.

PCF-based SPR sensors RI detection based on the CL. The loss peak and resonant frequency increases or decreases when RI changes.

3.3 Wavelength sensitivity

Wavelength sensitivity (WS) is one of the essential sensing parameters utilized in these specific sensors. It is calculated based on the wavelength sensitivity interrogation method. Eq. 5[42] is used to evaluate the WS.

$$S_l\left(\frac{nm}{RIU}\right) = \Delta l/\Delta n_a \quad \ldots(5)$$

Here, Δl denotes the change in resonant wavelength, and the change in RI is denoted by Δn_a.

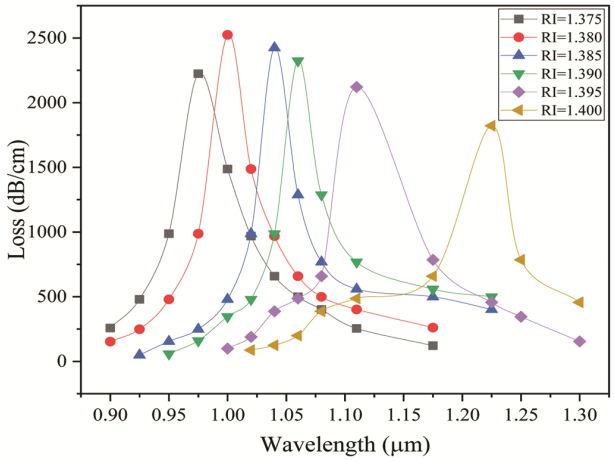

Fig. 3 — Confinement loss spectra vs operating wavelength for various RIs

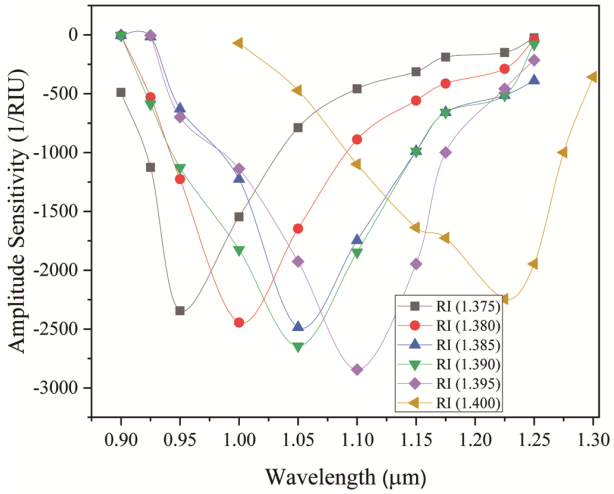

Fig. 4 — Amplitude sensitivity against operating wavelength for various RIs

This sensor detects RI for the range(1.375-1.400). The wavelength shifts are obtained by changing the RI from 1.375 to 1.400 with a step change of 0.005. For this investigation, the resonant wavelength is shifted by 114.3nm when the RI changes from 1.390 to 1.395. It illustrates that the maximum sensitivity obtained by this sensor is 22860 nm/RIU, determined by Eq. 5. As the RI changes increase, the ERI differences between the two guided modes are reduced, resulting in smooth coupling and sensitivity enhancement.

3.4 Analysis of confinement loss and amplitude sensitivity

The minor variation in RI causes a substantial decrease in the RI distinction between the SPP mode and core-guided mode. The loss spectra with loss peaks and resonant shifts obtained when RI varies from 1.375 to 1.400 are illustrated in Fig. 4. loss

spectra are obtained when the maximum light energy is focused in the cladding region in its place of the core region. Light coupling rises, interacting with the dielectric region through the material surface. Also, the coupling efficiency increases, resulting in a shift in resonant wavelength and loss peak shift towards higher wavelengths. Since amplitude sensitivity is highly reliant on the confinement loss value, sensitivity increases as the analyte RI value increases. When the RI of an analyte is 1.375, the loss peak and resonant wavelength are 2224 dB/cm and 0.975μm, respectively. Additionally, the corresponding RI of 1.380, 1.385, 1.390, 1.395 and 1.400 are 2524, 2224, 2321, 2120 and 1821 dB/cm loss peaks, respectively, and of 1, 1.04, 1.08, 1.11, 1.225 μm resonant wavelengths respectively. The RI of many biological cells, biochemicals, and harmful food additives are within the detected RI range (1.375-1.400). Adrenal gland cell cervical hela (RI 1.392) and PC-12 (RI 1.395)[43].

The average RI for infected red blood cells (RI 1.395) at the ring phase, several cancerous cells (breast cells- MDA -MB-231, RI 1.399), and blood cell-Jurkat (RI 1.390)[44]. Butyl acetate (RI 1.38) and tert-butyl alcohol (1.3878) are harmful food additives used for flavouring purposes in food processing[45]. These toxic chemicals, if not checked, can cause severe health hazards by dermal, oral, and breathing exposure[45]. The proposed sensor detects these mentioned chemicals. The amplitude sensitivity[46] is calculated using the amplitude sensitivity interrogation method using the relation illustrated in Eq. 6.

$$S_A(l) = -(1/\dot{\alpha}(l, n_a)\frac{\partial\dot{\alpha}(l,n_a)}{\partial n_a} \quad \ldots(6)$$

Here, the difference in loss peaks with n_a at wavelength, l is denoted by $\partial\dot{\alpha}(l, n_a)$, ∂n_a denotes the difference in RI, and $\dot{\alpha}(l, n_a)$ is the loss for n_a. The proposed sensor achieved the maximum AS of 1758 (1/RIU) at analyte RI 1.395. AS concerning operating wavelength for detected analytes is illustrated in Fig. 4. The value is also shown in Table 2. This parameter is generally used for sensing analyte properties at a particular wavelength.

3.5 Analysis of Confinement loss with variation in Silver layer thickness

The thickness of the plasmonic layers plays a vital role in designing PCF-based SPR sensors because the generation of SPPs and surface plasmonic waves (SPWs) highly depends on these layers. As the Silver layer thickness increases or decreases, the loss peaks change, but the resonant wavelength remains; hence, the wavelength sensitivity is not affected, but the amplitude will be changed. The thickness of the Silver layer varies from 60nm to 80 nm with a step change of 10nm. It is investigated that when the thickness of 80nm is used, the loss peaks decrease from 2324 dB/cm to 2121 dB/cm for RI variation from 1.390 to 1.395.

In this case, the proposed achieved the maximum RI compared to other RI variations because the thin plasmonic layer cannot accommodate a satisfactory number of SPP modes due to high damping. At the same time, a plasmonic layer that is too thick is also incapable of interrelating with an externally placed analyte due to limited infiltration depth and plasmonic damping. 80nm Silver layer emits many surface electrons and provides a more robust interaction of light energy with the analyte. The confinement loss spectra concerning wavelength for different thicknesses are illustrated in Fig. 5.

3.6 Variation of Ta_2O_5 layer thickness on confinement loss

In these specific sensors, improved sensitivity is required to detect the analytes accurately. Silver exhibits an oxidation problem in liquid chemical sensing. To avoid this issue and for better coupling the core mode with the SPP mode, a high-index Ta_2O_5 is utilized as an overlayer. The Ta_2O_5 thickness varies from 30nm to 40nm to investigate the effect on confinement loss and sensing performance. This variation causes the loss peak to decrease from 2324 dB/cm to 1875 dB/cm. Loss peaks and resonant wavelength also change by variation in thickness, resulting in wavelength and amplitude sensitivity changes, as illustrated in Fig. 6.

The confinement loss spectra concerning the operating wavelength for RI 1.390 are illustrated in

Table 2 — Comparison of proposed Ag-coated sensor with Au, Cu, and Al-coated sensors based on WS and AS when TiO_2 is utilized as a second plasmonic layer.

Materials	Refractive index range (RI)	Maximum wavelength sensitivity (nm/RIU)	Maximum amplitude sensitivity 1/RIU	ΔRI
Au-TiO_2	1.375-1.400	20000	1847	0.005
Ag-TiO_2	1.375-1.400	14600	1456	0.005
Cu-TiO_2	1.375-1.400	7600	464	0.005
Al-TiO_2	1.375-1.400	2520	223	0.005

Fig. 6. The thickness of 30nm with a Silver thickness of 80nm achieved the maximum sensitivities for the proposed sensor. Because on increasing the Ta_2O_5 thickness beyond 30nm, the light cannot interact with the analyte due to limited infiltration depth.

3.7 Fabrication feasibility

The values of each parameter greatly influence the total performance of the sensor. The well-known stack-and-draw fabrication approach can practically create the suggested sensor's circular core and cladding air holes. The stack-and-draw approach is the primary technique for creating PCFs worldwide. Nevertheless, there are minute flaws in the PCF fabrication process. Thus, minor adjustments to its characteristics may be conceivable. Constructing the gadget according to the precise design specifications can be challenging. Therefore, tolerance of ±3% or ±4% from the obtained characteristics is considered during fabrication. All the plasmonic materials layers are utilized circularly to avoid fabrication difficulty. These material coatings are fabricated by using chemical vapor deposition techniques.

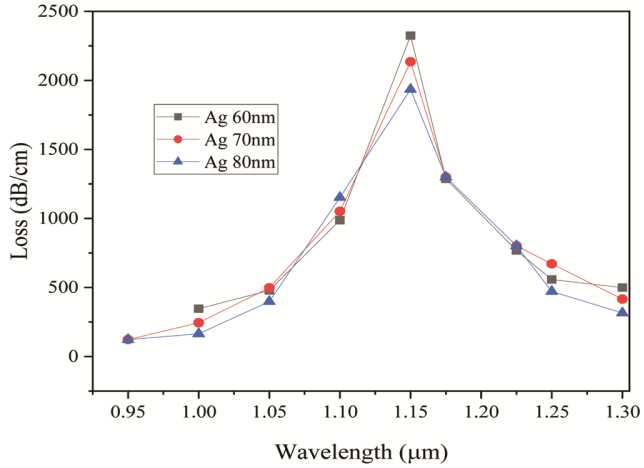

Fig. 5 — Confinement loss spectra for different Silver layer thicknesses at RI 1.390

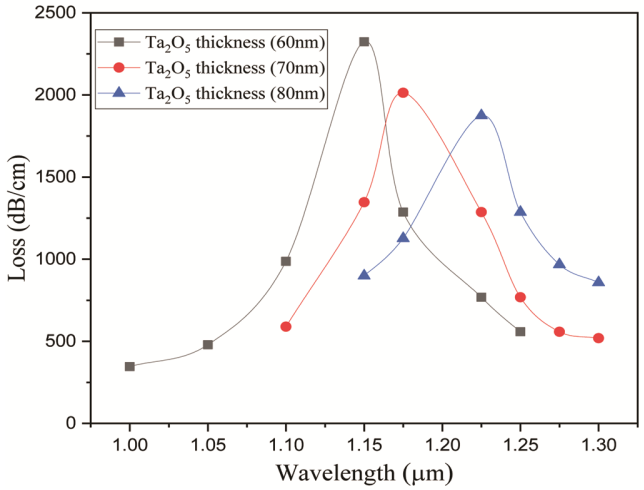

Fig. 6 — Effect of variation of Ta_2O_5 thickness on confinement loss at RI 1.390

3.8 Comparison of proposed Ag-coated sensor with Au, Cu, and Al-coated sensors

In this part, the Ag-coated sensor is first compared with Au, Cu, and Al-coated sensors when TiO_2 is utilized as the second plasmonic layer. Also, the effect of the Ta_2O_5 layer in place of the TiO_2 layer is investigated. The AS and WS parameters are used to examine the performance. Tables 3 and 4 illustrate the maximum AS and WS values obtained whenTiO_2 and Ta_2O_5 are used as second plasmonic layers. Fig. 7-10 illustrates the comparison graphically.

TiO_2 is a high-index material used to avoid Au adherence, emitting many surface electrons that efficiently draw the field from the core and permit strong interaction with the SPP mode, resulting in the sensing performance of Au-coated sensors. In the case of Ag and Cu, TiO_2provides stability in aqueous environment and smooth coupling but the effect is less than Au. Al does not achieved much attention in SPR sensing because of damping rate[47].

When the Ta_2O_5 layer is utilized as a second plasmonic layer, the Ag-coated sensor achieves better wavelength sensitivity than Au, Cu, and Al-coated sensors. Meanwhile, the coated sensor achieves the maximum amplitude sensitivity compared to others. Ag and Cu have sharper resonance peaks but are vulnerable to oxidation, causing low environmental stability[22]; the sensing performance of Ag and Cu-coated sensors degrades. To enhance the sensing

Table 3 — Comparison of proposed Ag-coated sensor with Au, Cu, and Al-coated sensors on based on WS and AS when Ta_2O_5 is utilized as a second plasmonic layer.

Materials	Refractive index range (RI)	Maximum wavelength sensitivity (nm/RIU)	Maximum amplitude sensitivity 1/RIU	ΔRI
Au-Ta_2O_5	1.375-1.400	21600	2248	0.005
Ag- Ta_2O_5	1.375-1.400	22860	1758	0.005
Cu- Ta_2O_5	1.375-1.400	10900	863	0.005
Al- Ta_2O_5	1.375-1.400	3240	314	0.005

Table 4 — Comparison of designed PCF-SPR sensors with some existing sensors.

Ref.	Year	Wavelength in nm	(RI) Detection range	Materials and design complexity	WS (nm/RIU)	AS (1/RIU)
[48]	2017	720-760	1.33-1.36	Gold- MoS_2	2000	200
[49]	2015	550-650	1.33-1.37	Gold	5200	216
[50]	2012	550-800	NA	Silver	7300	216
[51]	2017	1000-1600	1.43-1.46	Gold	7700	150
[52]	2017	560-740	1.33-1.37	Silver	4200	300
[53]	2019	1100-1300	1.385-1.400	TiN	10000	70
[54]	2020	2600-3600	1.30-1.38	ITO	10000	NA
[55]	2019	1500-2200	1.33-1.38	Gold-Graphene	4657.14	8600
[56]	2020	780-940	1.33-1.41	Silver	21000	2456
[57]	2019	700-840	1.33-1.40	Silver	12,000	1656
Au-TiO_2Designed Sensor	2022	900-1300	1.375-1.400	Gold-TiO_2	20000	1847
Ag-TiO_2 Designed Sensor	NA	900-1300	1.375-1.400	Silver-TiO_2	14600	1456
Au-Ta_2O_5 Designed Sensor	NA	900-1300	1.375-1.400	Gold-Ta_2O_5	21600	2248
Ag-Ta_2O_5 Designed Sensor	2023	900-1300	1.375-1.400	Silver-Ta_2O_5	22860	1758

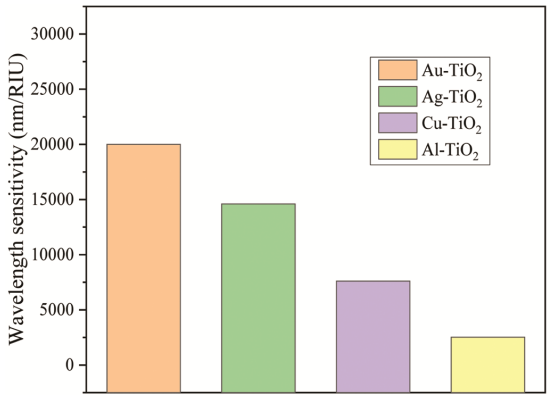

Fig. 7 — Comparison of WSs of Au, Ag, Cu, and Al coated sensor utilizing TiO_2 as a second plasmonic layer

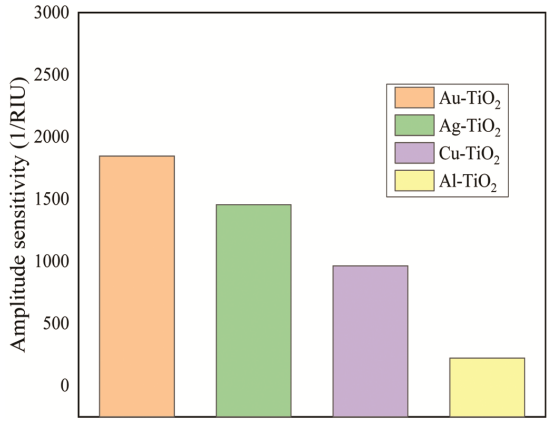

Fig. 8 — Comparison of ASs of Au, Ag, Cu, and Al coated sensors utilizing TiO_2 as a second plasmonic layer

capability of these sensors, a high refractive index material, Ta_2O_5, is coated as an overlayer to avoid oxidation. Ta_2O_5 has high environmental stability, provides better coupling between core mode and SPP

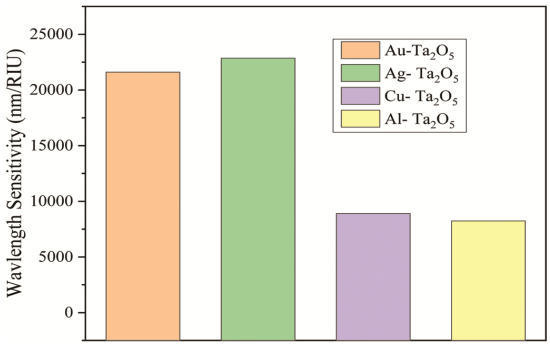

Fig. 9 — Comparison of WSs of Au, Ag, Cu, and Al coated sensor utilizing Ta_2O_5 as second plasmonic layer

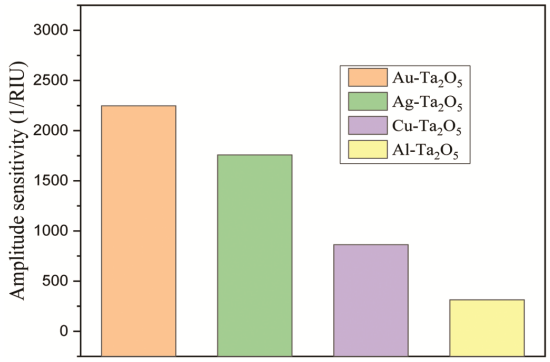

Fig. 10 — Comparison of ASs of Au, Ag, Cu, and Al coated sensor utilizing Ta_2O_5 as second plasmonic layer

mode, and is promising enough to increase the surface electrons of the Ag and Cu materials; in this way, these materials can be oxide-free, resulting in sensitivity enhancement.

On the other hand, Al, due to its high damping rate and optical losses, cannot generate substantial SPPs, resulting in low sensitivities. Among all these

materials, Au already exhibits high environmental stability; therefore, the effect of Ta_2O_5 is less on Au in aqueous conditions than on Ag and Cu. Ta_2O_5 makes the Ag oxide-free; in this way, Ag and Cu can generate more than sufficient plasmons. Also, Ta_2O_5 provides better coupling results in enhancing the sensing performance. We can design the low-cost Ag-Ta_2O_5 coated PCF-based SPR sensor by combining these materials.

4 Conclusion

In this paper, a low-cost Ag-Ta_2O_5 externally coated PCF-based sensor is proposed and numerically investigated. Plasmonic metal and analyte layers are created outside the fiber to simplify practical implementation. All the plasmonic material layers can be easily fabricated using chemical vapor deposition. All the circular airholes are used to simplify the fabrication, which can be achieved by the stack and draw procedure. This sensor is utilized to sense the analytes within the RI range of 1.375-1.400. The amplitude and wavelength sensitivities investigate the performance of the sensor; the investigation shows that AS of 1758 1/RIU and WS of 22860 nm/RIU are obtained by the proposed sensor for the thickness of Ag (80nm) and Ta_2O_5 (30nm) at RI 1.395. Additionally, the performance of the Ag-Ta_2O_5 coated sensor is compared withAu-Ta_2O_5, Cu-Ta_2O_5, and Al-Ta_2O_5 coated sensors and Ag-TiO_2, Au-TiO_2, Cu-TiO_2, and Al-TiO_2 coated sensors. The wide range (1.375-1.400) of RI detection abilities demonstrated by the proposed sensor solidifies it appropriate for a variety of biological and biochemical sensing applications; blood cells, cancerous cells, butyl acetate, and tert-butyl alcohol are the significant analytes this sensor can detect. Due to lowcost, fabrication simplicity, high sensitivity, wide detection range, and various sensing applications, this sensor can be utilized efficiently in PCF-based SPR sensing.

References

1 Konorov S O, Fedotov A B & Zheltikov A M, *Opt Lett*, 28 (2003) 1448.
2 Chow C-W, Kwok C H, Tsang H K & Lin C, *Opt Lett*, 31 (2006) 2535.
3 Mosley P J, Huang W C, Welch M G, Mangan B J, Wadsworth W J & Knight J C, *Opt Lett*, 35 (2010) 3589.
4 Revathi S, Sigedar V P, Chourasia A, Landge M & Gulawani A, *Indian J Sci Technol*, (2016).
5 Akimov D, T. Siebert, W. Kiefer, and A. Zheltikov, *JOSA B*, 23 (1988) 2006.
6 Xing Z, Huang B, Xue L, Cao J & Lou S, *Infrared Phys Technol*, 124 (2022) 104212.
7 Cubillas A M, *et al.*, *Chem Soc Rev*, 42 (2013) 8629.
8 Ademgil H & Haxha S, *Sensors*, 15 (2015) 31833.
9 Jain S, Choudhary K & Kumar S, *Opt Fiber Technol*, 73 (2022) 103030.
10 Otto A, *Zeitschrift für Phys A Hadron Nucl*, 216 (1968) 398.
11 Kretschmann E & Raether H, *Zeitschrift für Naturforsch A*, 23 (1968) 2135.
12 Gupta B D, Verma R K, *et al*., *J Sensors*, 2009 (2009).
13 Zhao Y, Deng Z & Li J, *Sens Actuators B Chem*, 202 (2014) 557.
14 Gupta B D & Sharma A K, *Sens Actuators B Chem*, 107 (2005) 40.
15 Singh S, Mishra S K & Gupta B D, *Sens Actuators A Phys*, 193 (2013) 136.
16 Elsherif M, *et al.*, *Adv Photon Res*, 3 (2022) 2100371.
17 Fatema S, Absar R, Reja M I & Akhtar J, *IEEE Int Conf on Telecommun Photon (ICTP)*, (2017) 1.
18 Ramola A, Marwaha A & Singh S, *Appl Phys A*, 127 (2021) 643.
19 Liang H, Feng Y, Liu H, Han W & Shen T, *Plasmonics*, 17 (2022) 1765.
20 Siddik M A B, Hossain M S, Paul A K, Rahman M M, Roni M H K & Chakrabatri K, *IEEE Region 10 Symposium (TENSYMP)*, (2020) 1795.
21 Danlard I & Akowuah E K, *Opt Fiber Technol*, 54 (2020) 102083.
22 Dash J N & Jha R, *IEEE Photon Technol Lett*, 26 (2014) 595.
23 Shakya A K, Ramola A, Singh S & Van V, *Opt Express*, 30 (2022) 9233.
24 Liu W, *et al.*, *Results Opt*, 1 (2020) 100004.
25 Rifat A A, Hasan M R, Ahmed R & Butt H, *Nanophoton*, 12 (2018) 12503.
26 Shafkat A, *Sens Bio-Sensing Res*, 28 (2020) 100324.
27 Kadhim R A, Yuan L, Xu H, Wu J & Wang Z, *IEEE Sens J*, 20 (2020) 9816.
28 Singh S & Prajapati Y K, *Optik (Stuttg)*, 224, (2020) 165525.
29 Ibrahimi K M, Kumar R & Pakhira W, *Optik (Stuttg)*, 288 (2023) 171186.
30 Hasan M S, Kalam M A E & Faisal M, *IEEE Trans. Nanobioscience*, (2023).
31 Dash J N & Jha R, *IEEE Photon Technol Lett*, 26 (2014) 1092.
32 Wang Y, Jiang G, Yu Z, Wang Q & Jiang X, *Sens Bio-Sens Res*, 34 (2021) 100452.
33 Bourdine A V, *et al.*, *Fibers*, 9 (2021) 27.
34 Singh S, Chaudhary B, Upadhyay A, Sharma D, Ayyanar N & Taya S A, *Photon Nanostruct-Fundament Appl*, (2023) 101119.
35 Islam M R, *et al.*, *Optik (Stuttg)*, 221 (2020) 165311.
36 Kumar S & Kumar D, *MAPAN*, 37 (2022) 435.
37 Das S, *Photon Nanostruct-Fundament Appl*, 44 (2021) 100904.
38 Yang H, *et al.*, *Sensors*, 21 (2021) 818.
39 Islam M R, *et al.*, *Plasmonics*, 16 (2021) 849.
40 Rifat A A, *et al.*, *Sens Actuators B Chem*, 243 (2017) 311.
41 Liu C, *et al.*, *IEEE Photon Technol Lett*, 30 (2018) 1471.
42 Wang F, Sun Z, Liu C, Sun T & Chu P K, *Opto-Electron Rev*, 26 (2018) 50.
43 Abdelghaffar M, *et al.*, *Opt Quant Electron*, 55 (2023) 472.

44 Chaudhary V S, Kumar D & Kumar S, *IEEE Sens J*, 21 (2021) 17800.
45 Atiqullah S M, Palit A, Reja M I, Akhtar J, Fatema S & Absar R, *Sens Bio-Sens Res*, 23 (2019) 100275.
46 Li W, Chen Y, Xu J, Jiang M & Zou H, *Micromachines*, 14 (2023) 1295.
47 West P R, Ishii S, Naik G V, Emani N K, Shalaev V M & Boltasseva A, *Laser Photon Rev*, 4 (2010) 795.
48 Nivedha S, Babu P R & Senthilnathan K, *IOP Conf Ser: Mater Sci Eng*, 263 (2017) 52031.
49 Luan N, Wang R, Lv W & Yao J, *Opt Express*, 23 (2015) 8576.
50 Tian M, Lu P, Chen L, Lv C & Liu D, *Opt Commun*, 285 (2012) 1550.
51 Gangwar R K & Singh V K, *Plasmonics*, 12, (2017) 1367.
52 Momota M R & Hasan M R, *Opt Mater (Amst)*, 76 (2018) 287.
53 Kaur V & Singh S, *Opt Fiber Technol*, 48 (2019) 159.
54 Kaur V & Singh S, *Optik (Stuttg)*, 220 (2020) 165135.
55 Lou J, Cheng T, Li S & Zhang X, *Opt Fiber Technol*, 50 (2019) 206.
56 Hossain M B, Islam S M R, Hossain K M T, Abdulrazak L F, Sakib M N & Amiri I S, *Results Phys*, 16 (2020) 102909.
57 Mahfuz M Al, *et al*, *Opt Mater (Amst)*, 90 (2019) 315.